Solar Energy 287 (2025) 113230

Contents lists available at ScienceDirect

Solar Energy

journal homepage: www.elsevier.com/locate/solener

Thermal emittance measurement of low-emissive materials for enhanced conversion efficiency in vacuum-based solar thermal applications

Eliana Gaudino [a,b], Umar Farooq [b,c], Antonio Caldarelli [b], Paolo Strazzullo [a,b], Daniela De Luca [b,c,1], Emiliano Di Gennaro [b,c], Roberto Russo [b,*], Marilena Musto [a,b]

[a] Industrial Engineering Department, University of Napoli "Federico II", Piazzale Vincenzo Tecchio, 80 80125, Napoli, Italy
[b] Institute of Applied Sciences and Intelligent Systems, National Research Council of Italy, via Pietro Castellino 111 80131, Napoli, Italy
[c] Physics Department, University of Napoli "Federico II", Via Cinthia, 21, Napoli 80126, Italy

ARTICLE INFO

Keywords:
Thermal emittance
Calorimetric measurements procedure
Selective solar absorbers
High vacuum flat plate collectors
Very low thermal emittance

ABSTRACT

In the quest for more efficient solar thermal systems, accurately determining the thermal emittance of low-emissive materials is crucial in determining the power losses. This paper describes the calorimetric method designed to precisely measure the thermal emittance of Selective Solar Absorbers (SSAs) to be used in High Vacuum Flat Plate Collectors (HVFPCs). The method's capability is demonstrated through the successful correction of thermal emittance values for copper samples of varying sizes, including dimensions down to 49 cm2. Results highlight the method's potential to significantly reduce measurement errors associated with small-size and/or low-emittance samples, providing a path forward to improve the design and efficiency of SSAs. This research marks a significant step in advancing solar thermal technology by enabling emittance measurements with a precision better than 0.003, which is essential for the development of high-performance solar thermal absorbers. The method has also been applied to correct the thermal emittance value of SSA measured in previous measurement campaigns, and it allows a better estimation of the SSA efficiency conversion curve.

1. Introduction

Thermal emittance is a fundamental property that quantifies the radiant energy a surface emits in comparison to an ideal blackbody at the same temperature. It plays a pivotal role in assessing the energy transfer and efficiency of thermal systems, such as solar absorbers [3,13], building insulation materials[8,14], and heat exchangers[17].

Selective solar absorbers (SSAs) have gained significant interest in recent years due to their potential to enhance the efficiency and performance of solar thermal systems. For vacuum-based collectors, optimizing the thermal emittance is essential to achieve high conversion efficiency and minimize energy losses through thermal radiation[4,9].

SSAs are designed to absorb solar radiation selectively while minimizing thermal radiation losses. They should exhibit high solar absorption capability within the solar spectrum ($\lambda = 0.3$–2.5 μm) and low emissivity in the infrared (IR) region ($\lambda > 2.5$ μm) in order to preserve the absorbed solar energy within the system. This feature is especially vital for high-vacuum flat plate collectors (HVFPCs), where reducing thermal losses due to emitted power is crucial for maintaining high stagnation temperatures and achieving optimal energy conversion efficiency.

The efficiency of a Selective Solar Absorber (η_{SSA}) is defined as the ratio of the collector's useful heat output (Q_h) to the total solar irradiance incident on the absorber (G_{Sun}), adjusted by a concentration factor (C) that accounts for any reflectors present. This relationship can be expressed by the formula:

$$\eta_{SSA} = \frac{Q_h}{G_{sun}C} = \alpha - w^*\varepsilon \tag{1}$$

In this equation, η_{SSA} is also represented as a combination of the solar absorptance (α) and thermal emittance (ε), weighted by a factor (w) defined as the ratio of the maximum exchangeable heat through radiation with the ambient environment at temperature (T_{amb}) to the solar irradiance incident on the absorber, adjusted by the concentration factor (C):

$$w = \frac{\sigma_{SB}{}^*\left(T_{abs}^4 - T_{amb}^4\right)}{G_{sun}C} \tag{2}$$

* Corresponding author.
E-mail address: roberto.russo@na.isasi.cnr.it (R. Russo).
[1] Present address: Energy Research Institute at Nanyang Technological University, 50 Nanyang Drive, Singapore.

https://doi.org/10.1016/j.solener.2024.113230
Received 2 May 2024; Received in revised form 22 November 2024; Accepted 27 December 2024
Available online 3 January 2025

Nomenclature

A	surface (cm^2)
c_p	heat capacity (J/kgK)
ε	Thermal emittance
σ	Stefan-Boltzmann constant (W/m^2K^4)
m	Mass (kg)
z_1	Additional radiative thermal loss coefficient
z_2	Additional conductive thermal loss coefficient

Abbreviations

ATL	Additional Thermal Losses
MTB	Mini Test Box

Subscripts

s	Sample
th	Thermocouple

In essence, w quantifies how significant the emission mechanism is compared to light absorption.

This weighting factor (w) depends on the concentration factor and increases with absorber temperature. Notably, for a flat collector ($C = 1$) operating above 130 °C, w exceeds 1, indicating that thermal emittance becomes more critical than solar absorptance in determining absorber performance. Very low emissive SSA are therefore needed to reach high efficiencies at higher temperatures in HVFPC and a precise knowledge of the thermal emittance at the operating temperature is essential for a correct estimation of the conversion efficiency.

The exploration of novel materials has opened new pathways for improving SSAs performances[35]. One effective method for producing SSAs suitable for high-temperature solar thermal applications involves the incorporation of metal nanoparticles within a dielectric matrix, resulting in materials known as cermets. Numerous cermet-based absorbers have been developed, such as the stable cermet composed of conductive titanium nitride (TiN) embedded in silica (SiO_2), which demonstrates an absorptance of 0.92 even after undergoing annealing at 650 °C, with a thermal emittance of 0.18[5]. Additionally, the optimization of a platinum-alumina (Pt-Al_2O_3) double cermet SSA achieved remarkable results, obtaining a solar absorptance of 0.97 and a thermal emittance of just 0.05[20].

Another prevalent structure for SSAs consists of multilayer films that create multiple interfaces along the light path[30]. For instance,[15] proposed a near-ideal solar absorber comprising a nickel (Ni) nanowire array combined with a multilayer system of titanium dioxide (TiO_2), tungsten (W), and silica (SiO_2), achieving over 90 % optical absorption across a wavelength range of 300 to 1900 nm. The inherent complexity of multilayer structures necessitates thorough characterization to comprehend how variations in layer properties affect overall efficiency. Spectrally selective solar absorbers, designed as $Cr/Cr_2O_3/Cr/Cr_2O_3/SiO_2$ configurations, were developed specifically for high vacuum flat-plate collectors (HVFPCs) [11]. An optimization algorithm was employed to create multilayer SSAs suitable for mass industrial production, yielding solar absorptance values as high as 0.97 and thermal emittance below 0.05, even at temperatures up to 300 °C.

Ongoing research in the HVFPC field aims not only to reduce thermal emittance on the front side of the absorber but also to minimize power emitted from the back side towards the panel bottom case by developing selective solar absorbers (SSA) on low-emissive coated substrates[3].

Copper (Cu) is a highly promising material for low-emissive SSA substrates, as it exhibits extremely low thermal emittance ($\varepsilon < 0.02$)[23] also in the form of thin films[22].

Developing SSAs with excellent optical properties requires reliable and precise measurements of emissivity. However, accurately determining the emissivity of coatings can be challenging due to the influence on the measurements of optical properties, surface roughness [18,27,34], and composition[28–29]. Additionally, environmental conditions, such as temperature and humidity, may also affect the accuracy of thermal emittance measurements[31,32–33].

Several methods are commonly used to measure the thermal emittance of coatings, including spectroscopic methods, such as infrared reflectometry and Fourier-transform infrared spectroscopy (FTIR)[26], as well as calorimetric methods[6], such as the heat flux meter[1]or radiometric measurements[19]. Each method has its advantages and limitations, and the choice of technique depends on the specific requirements of the measurement and the properties of the coating being evaluated.

Thermal emittance measurements for selective solar absorbers (SSAs) are typically performed at room temperature and near-normal incidence angles, as documented in recent literature[21]. This approach offers a reasonable estimate, assuming that the optical properties are not substantially affected by temperature or angle of incidence. In our study, we aim to overcome these limitations by using calorimetric techniques to measure the hemispherical emittance of SSAs across a range of temperatures.

Calorimetric techniques provide valuable insights into the coating's radiative properties, measuring the heat flux emitted by the coating under controlled conditions.

In the context of Selective Solar Absorbers (SSAs) used in High Vacuum Flat Plate Collectors (HVFPCs), the total hemispherical emissivity measurement method using a calorimetric technique was first reported by[25]and then described in detail in[7].

This method utilizes a specialized test equipment called from here on Mini Test Box (MTB), designed to replicate HVFPC conditions. Previous work has successfully applied the MTB apparatus to measure the total hemispherical emittance of selective absorbers with an Aluminum substrate and a surface area of 210 cm2[7]. For the experimental conditions reported in[7], it is demonstrated that all the thermal losses not related to the sample thermal radiation are negligible and that the cooling down of the sample under test can be attributed entirely to sample radiated power, providing an accurate measurement of the thermal emittance for the sample under test. The correct assessment of the SSA thermal emittance allows for the correct evaluation of the energy conversion efficiency in HVFPCs as recently demonstrated by[12].

However, when dealing with SSAs having very low thermal emittance and/or smaller dimensions, the thermal power emitted from the sample surfaces decreases, and other contributions to the sample cooling down can no longer be neglected, and their impact on the thermal emittance measurements needs to be evaluated.

This manuscript experimentally evaluates the thermal losses other than the radiative power emitted by the sample. These Additional Thermal Losses (*ATL*) are evaluated by measuring Cu samples cut with different dimensions from the same copper foil. The *ATL* evaluation enables the thermal emittance measurements for copper samples with a minimal dimension of 49 cm^2 in agreement with the literature data.

The manuscript also provides insight into steps required to further reduce the sample size and/or achieve lower measurable values of thermal emittance, thereby enabling accurate measurement of low emittance SSA as required by HVFPCs. Furthermore, the *ATL* losses can be subtracted from SSA measurements performed in the same conditions, allowing the correction of thermal emittance values reported in our previous papers.

2. Measurement procedure

The experimental setup for the SSA sample's emissivity measurements, considered in this manuscript is depicted in Fig. 1 and it is routinely used to assess the SSA properties also during aging tests [2].

It consists of a rectangular stainless steel vacuum chamber (n° 1 in Fig. 1) sealed by a removable glass cover (n°2 in Fig. 1). A vacuum seal is

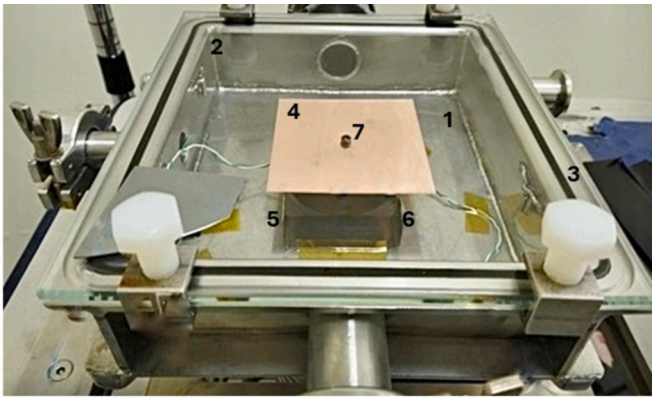

Fig. 1. Photograph of the MTB Experimental Apparatus: The copper absorber sample is mounted inside the MTB Vacuum Chamber for measurements. The numbers in the figure correspond to the main components of the MTB apparatus (see text for details).

achieved using a Viton O-Ring (n°3 in Fig. 1), which is compressed by the glass plate. The chamber operates under a high-vacuum regime obtained through a turbo-molecular pumping system. Flat absorber samples (n°4 in Fig. 1), with a maximum dimension of 210 cm^2 (14 cm x 15 cm), are placed inside the vacuum chamber.

The procedure involves obtaining a calorimetric measurement of temperature-dependent thermal emittance by monitoring the instantaneous temperature variation of the sample during the cooling phase after it has been heated to stagnation temperature by the LED system's irradiated power.

The temperatures of the sample, cover glass, and chamber walls are measured using K-type thermocouples and read out using a USB module (National Instruments 9211). The sample thermocouple is crimped to a lug and screwed to the central hole of the sample using an M3 stainless steel nut and bolt (n°7 in Fig. 1). The glass and chamber temperature sensors are placed on the vacuum side to ensure that the external air convection, whether natural or forced, does not affect the temperature measurements.

In this case, the calorimetric equation used to obtain the thermal emittance of the sample under analysis can be written, under some approximations, as follows:

$$\left[m_s c_{ps}(T_s) + m_{th} c_{pth}(T_s)\right] \frac{dT_s}{dt} = -2\varepsilon_s(T_s) A_s \sigma \left(T_s^4 - T_{box}^4\right) \tag{3}$$

where m_s, A_s and $c_{ps}(T_s)$ represent the mass, the surface and the temperature-dependent heat capacity of the analyzed sample respectively; m_{th} and $c_{pth}(T_s)$ are the mass and the temperature-dependent capacity of the sample thermocouple fastening bolt and nut; T_s, and T_{box} *(K)* denote the sample temperature and the average temperature of glass and vessel of the MTB vacuum chamber, respectively, while σ is the Stefan- Boltzmann constant. ε_s represents the thermal emittance of the sample that is the objective of the measure and the factor 2 indicates that the upper and lower surfaces of the samples have the same thermal emittance.

Other causes of thermal losses are explicitly ignored in this approach and they are reported at beginning of section 2.1.

The reliability of thermal emittance measurements during the cooling phase is limited by experimental noise. The more the sample temperature decreases, the more the measured temperature variation per unit of time becomes comparable to the thermocouple resolution, resulting in increased error and noise. A moving average of the measured data is used to reduce noise, and a linear (first-order) fit is applied to represent the total thermal emittance of the sample. As discussed in[7], to obtain reliable measurements, the data acquisitions are recorded from stagnation temperature down to a minimum absorber temperature of 100 °C; a temperature region where the sample power dissipated by thermal radiation is more than one order of magnitude higher than the other thermal exchange mechanisms and justify the assumption made in Equation (3).

However, for cases where the sample emitted power during the cooling phase is not sufficiently high to disregard these other heat exchange mechanisms, it is crucial to account for them. These additional mechanisms arise from the interaction between the elements of the experimental setup and the sample under analysis. When dealing with very low-emissive materials or samples with dimensions smaller than 210 cm^2, neglecting these additional thermal losses can lead to non-negligible errors in the thermal emittance value of the analyzed sample.

2.1. Calorimetric balance equation for very low-emissive materials

The factors that contribute to the the sample cooling and neglected in the calorimetric Equation (3) can be critical for accurately determining the thermal emittance of low-emissive materials as sample size decrease. In particular the sample is supported by some stainless steel springs in the vacuum chamber and it experiences conductive cooling by these supports. The thermocouple, attached via an M3 bolt to the sample's center, contributes to the cooling due to its conductive and radiative properties.

For a more precise measurement it's necessary to revise the calorimetric equation (Equation (3) to include these considerations.

$$\left[m_s c_{ps}(T_s) + m_{th} c_{pth}(T_s)\right] \frac{dT_s}{dt} = -2\varepsilon_s(T_s) \sigma A_s \left(T_s^4 - T_{box}^4\right) - ATL(T_s, T_{box}) \tag{4}$$

In this equation, the term *ATL* (T_s, T_{box}) represents the Additional Thermal Losses and accounts for the fraction of the cooling power exchanged due to the heat transfer mechanisms mentioned above and neglected in Equation (3). In the study by[7], the negligibility of *ATL* for large area samples was estimated and demonstrated; however, the development of a precise model to evaluate such losses with the accuracy required for their subtraction in Equation (4) proved to be unfeasible. Consequently, we have opted for an experimental evaluation of these losses, as detailed in the following section.

2.2. Procedure for quantification of the additional thermal losses function

The inclusion of the *ATL* (T_s, T_{box}) term in the thermal balance adds an unknown term to Equation (4) other than $\varepsilon_s(T_s)$. Hence it becomes imperative to ascertain the functional expression for additional thermal losses in order to solve the complete calorimetric equation.

To determine the *ATL* expression, the adopted methodology involves measuring at least two samples possessing identical thermal emittance but varying in dimensions. Under these circumstances, the thermal emittance can be derived by assuming that the *ATL* remains consistent across these different measurements. These assumptions, which will be subsequently validated by measuring a larger set of samples, enable the determination of both the thermal emittance and the *ATL* term by solving a system of two equations with two unknowns:

$$\begin{cases} \left[m_{s1} c_{ps}(T_s) + m_{th} c_{pth}(T_s)\right] \dfrac{dT_s}{dt} = -2\varepsilon_s(T_s) \sigma A_{s_1} \left(T_s^4 - T_{box}^4\right) - ATL(T_s, T_{box}) \\ \left[m_{s2} c_{ps}(T_s) + m_{th} c_{pth}(T_s)\right] \dfrac{dT_s}{dt} = -2\varepsilon_s(T_s) \sigma A_{s_2} \left(T_s^4 - T_{box}^4\right) - ATL(T_s, T_{box}) \end{cases} \tag{5}$$

In Equation (5), the subscripts 1 and 2 indicate that the two samples have different areas and different masses; all the other parameters are assumed to be identical.

The subsequent section will present the outcomes obtained from bulk copper samples of distinct dimensions. Calorimetric measurements were performed on four squared bulk copper samples having different surface areas. For each pair of samples composed of the same material but

exhibiting different dimensions, the system of Equation (5) was solved, considering that when the sample and box temperatures (T_s, T_{box}) are identical, the thermal emittance ε_s should be the same. The reduction process occurring in copper oxides under high vacuum conditions at 300 °C[16]is crucial to ensure the absence of oxidation on the sample surfaces, which, in turn, guarantees the same thermal emittance among the samples.

For the set of four samples with different dimensions under analysis, six possible combinations of two elements arise. Solving the system (Equation (5) for these six distinct combinations yields six $ATL(T_s)$ curves, which will be presented and discussed in the ensuing section.

3. Results

Fig. 2 shows the results of thermal emittance measurements conducted on bulk copper (Cu) samples of various dimensions (210 cm^2, 100 cm^2, 64 cm^2, and 49 cm^2), obtained neglecting the *ATL* contribution in the calorimetric balance equation (Equation (3). Despite being the same material, different sample sizes analyzed by Equation (3) return different thermal emittance values.

Samples show a pronounced effect of additional thermal losses that, if not considered, lead to an overestimated thermal emittance, especially in smaller samples. Fig. 2 b) shows the results of the fitting procedure on the raw data presented in Fig. 2 a).

The trend of *ATL* was obtained by determining the copper samples cooling power during the calorimetric measurements and resolving the system of Equations (5).

Fig. 3 displays the *ATL* curves (continous lines) as a function of the absorber sample temperature.

The variations in box temperature with respect to T_s were negligible during the measurements of samples of different dimensions. Thus, the *ATL* function is only represented with respect to the sample temperature.

In the legend of the graph, each curve is indicated by the dimensions (in cm^2) of the pair of samples whose balance equation is coupled in the system (5). The *ATL* obtained are very similar, with a maximum variation of less than 10 % with respect to the average, supporting the hypothesis that *ATL* does not depend on the sample dimensions but only on its temperature. Under this hypothesis, the average curve was calculated (dashed black line in Fig. 3) and considered to obtain the function to be incorporated into the complete calorimetric balance equation (Equation (4).

Considering that the apparatus works in high vacuum, we can safely assume[12] that the additional thermal losses consist of two terms: a radiative term due to different thermal emittance of bolt and nut, proportional to the fourth power difference between the sample and box temperatures according to the Stefan-Boltzmann law, and a conductive term, proportional to the temperature difference between the sample and box. The *ATL* expression can be assumed to have the following form:

$$ATL(T_s, T_{box}) = z_1 * (T_s^4 - T_{box}^4) + z_2 * (T_s - T_{box}) \quad (6)$$

For copper (Cu) samples the coefficients z_1 and z_2 are obtained by fitting the experimental average ATL (T_s, T_{box}) curve shown in Fig. 3 a) to Equation (4).

The *ATL* expression for copper samples in the present configuration is:

$$ATL(T_s, T_{box}) = 4.2E-12 * (T_s^4 - T_{box}^4) + 7.4E-4 * (T_s - T_{box}) \quad (7)$$

Using the previous expression of *ATL* (T_s, T_{box}), Equation (4) can now be used to calculate the thermal emittance curves for the copper samples: the results are reported in Fig. 3 b). These curves overlap with each other and with the copper hemispherical emissivity curve found in the literature [24] (also reported in Fig. 3 b)) at high temperatures and differ by less than 0.003 at 150 °C.

4. Discussion

Once the expression for the *ATL* function (ATL (T_s, T_{box})) is obtained for copper samples, it is possible to compare the magnitude of losses introduced by the MTB experimental setup to the emitted power from samples of various dimensions. This comparison allows us to determine when it is possible to neglect the ATL term in the calorimetric balance equation as, for instance, it was correctly done in [7]. Furthermore, it helps to identify situations where, despite considering the *ATL* term, its significant influence on the measurements prevents the accurate deduction of the sample's emitted power from the total thermal losses.

4.1. Weight of additional thermal losses on measurements: Assessing the influence of sample temperature, dimension, and thermal emittance

Fig. 4 represents the ratio between *ATL* and the sample emitted power (both calculated in watts) as a function of the absorber temperature for samples of different areas. A ratio of 1 indicates that the losses induced by the experimental setup match the power emitted by the sample during a cooling phase, and reliable measurements can be obtained for a ratio below 1. Fig. 4 illustrates that with the current configuration, considering the *ATL* term in the calorimetric balance equation, it is possible to assess the thermal emittance of copper samples with dimensions higher than 49 cm^2 at temperatures higher than 150 °C: copper samples having an area smaller than 49 cm^2 have *ATL* comparable to/or larger than the emitted power from the sample, making the measurement too influenced by the subtraction of these additional dissipations.

It is interesting to observe that the ratio reported in Fig. 4 reduces with temperature, meaning that the measurement is more reliable at high temperatures. At a fixed temperature of the sample, the *ATL*/emitter power ratio can be graphically represented as a function of the

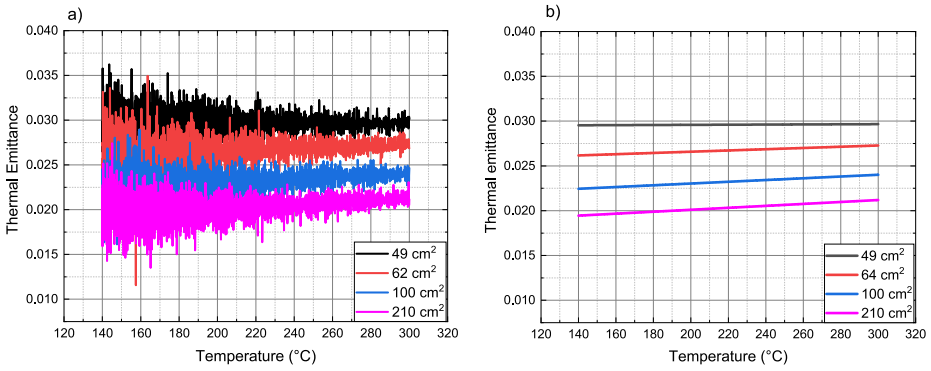

Fig. 2. a): thermal emittance as a function of the sample temperature for copper samples having different dimensions calculated according to equation(3); b): Linear regression of the data reported in a).

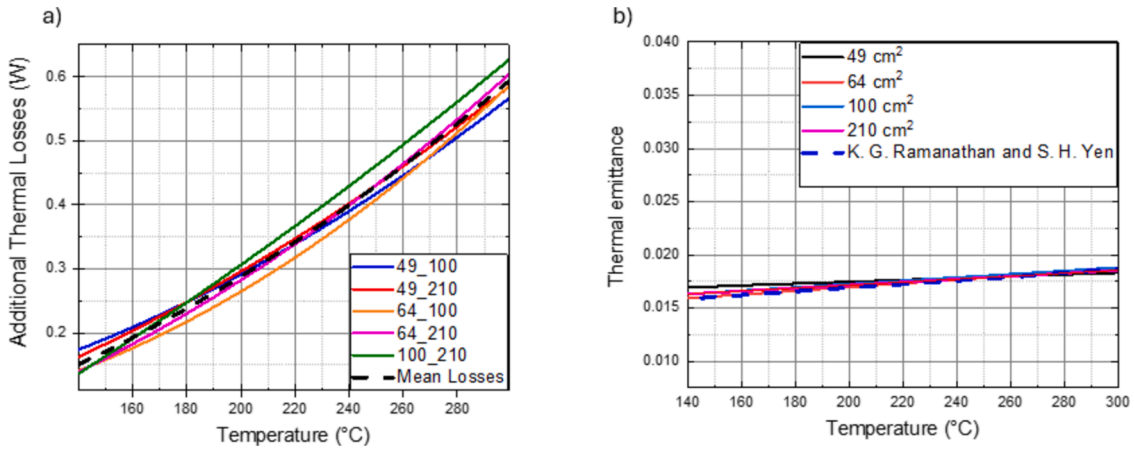

Fig. 3. a) measured additional thermal losses curves (colored continuous lines) as function of the sample temperature: the legend reports the two dimensions (in cm^2) used in Equation (3) to calculate the ATL. The average ATL curve is reported as dashed black line;3b): Thermal emittance of copper samples with different dimensions (210, 100, 64, 49 cm^2) according to Equation (2) and (5) (continuous lines). The dashed blue line represents the literature data of Copper thermal emittance reported in [24]. (For interpretation of the references to color in this figure legend, the reader is referred to the web version of this article.)

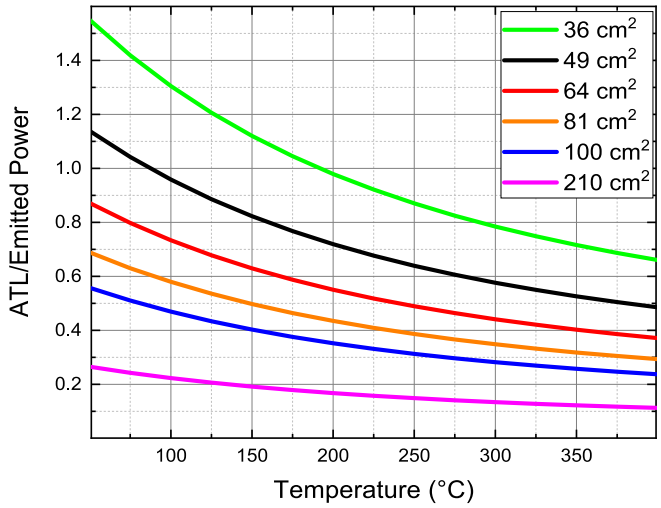

Fig. 4. Ratio between *ATL* and sample emitted power as a function of temperature for Copper samples of varying dimensions from 36 to 210 cm^2 (see legend).

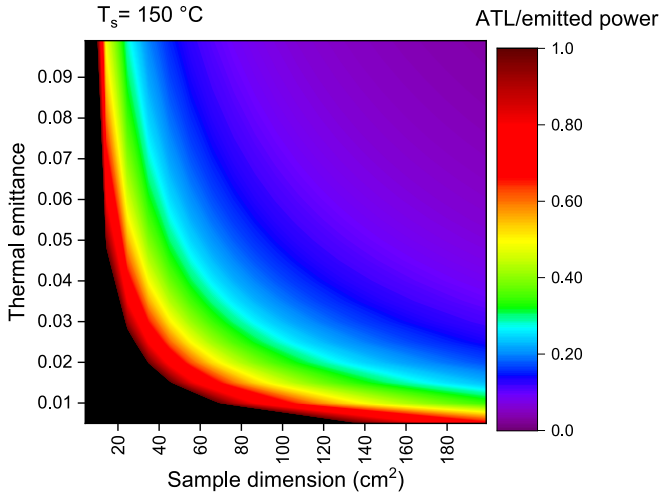

Fig. 5. Ratio of between *ATL* and copper sample emitted power at a fixed T_s = 150 °C a function of the dimension of the sample under analysis in cm^2 (X axis) and sample thermal emittance (Y axis). The region where the ratio *ATL*/emitted power is higher than 1 is plotted in black.

sample dimension and thermal emittance and used to establish the minimum dimension that can be correctly measured for a given thermal emittance.

The results for a temperature of 150 °C are depicted as a color map in Fig. 5. In samples with dimensions larger than 200 cm2 and a thermal emittance at 150 °C exceeding 0.09, represented by the violet region in the colormap (similar to the samples tested in[7], the ratio of *ATL* to emitted power is approximately zero. This indicates that the *ATL* term can be disregarded in the calorimetric balance equation. However, as the sample dimensions and/or the thermal emittance decrease, the colormap transitions into the green, yellow, and red regions, pointing out a greater impact of *ATL* in the sample cooling process. The black region in Fig. 5 denotes the scenario where the *ATL*/emitted power ratio exceeds 1.

Fig. 5 is crucial for understanding the minimal thermal emittance that can be accurately measured using samples of specific dimensions as delineated in Equations (4) and (7). For samples with a copper substrate, accurate evaluation of thermal emittance is feasible within the violet, blue, and yellow regions of the colormap. Considering the *ATL*, to measure thermal emittance values lower than 0.02 samples measuring 40 cm^2 cannot be used.

The correct determination of the *ATL* term is pivotal for thermal emittance measurements by the calorimetric method for SSA deposited on copper, which in turn is essential to assess the radiative losses in SSA and their solar energy conversion efficiency as described in the next subsection.

4.2. *Correction of measured thermal emittance of selective solar absorbers deposited on bulk copper substrate*

The calorimetric equation in the case of SSA deposited on copper contains two radiative terms for the two sample surfaces: the SSA and the copper substrate. The thermal emittance of the substrate and the *ATL* can be accurately measured using the method described in this paper and the only unknown in the calorimetric equation remains the thermal emittance of the SSA under measurement.

In[11]it was presented a novel approach to SSA design and optimisation based on a genetic algorithm and Cr_2O_3 and Cr multilayers. These SSAs were meticulously designed to enhance the efficiency of solar-to-thermal conversion at intermediate temperatures within an HVFPC

and deposited by sputtering.

Two optimized configurations of SSA samples, denoted as coating A (optimized for operation at 200 °C) and coating B (optimized for operation at 300 °C), were deposited on copper substrates with a dimension of 100 cm^2 [10]. The thermal emittance of the SSAs was measured using the MTB apparatus, and the absorber efficiencies were evaluated under specific conditions: solar irradiance of 1000 W/m^2 and an ambient temperature of 20 °C (Eq. (5) in [10]. The measured thermal emittance values, depicted in Fig. 6 a) with dashed lines, were compared to those of a commercial absorber (represented by the black line). However, the measured thermal emittance of the SSAs was approximately 0.04 higher than the values predicted by simulations for both multilayers.

This high discrepancy between the expected and measured thermal emittance values for coating A and B was unclear. It can now be attributed to the neglect of *ATL* influence in evaluating thermal emittance by solving Equation (3). To address this issue, incorporating the expression of *ATL* (T_s, T_{box}) specifically for samples with copper substrates, the thermal emittance values for coating A and B were reassessed and are presented in Fig. 6 a) as continuous lines. These reassessed values were utilised to compute the absorber efficiency displayed in Fig. 6 b) according to Equation (1). Fig. 6b) highlights the importance of the thermal emittance evaluation at temperatures higher than 150 °C, leading to about a 10 % efficiency increase at 300 °C for both samples.

The discrepancy between the simulated thermal emittance values and the measured values reported in Fig. 6a) was significantly reduced to 0.025. The remaining deviation can be attributed to the presence of layer thickness variation on a large-area sample. In fact, the SSAs are usually deposited using Phisycal Vapor Deposition(PVD) techniques such as magnetron sputtering, and a good layer thickness uniformity is obtained on an area that is a fraction of cathode dimensions (10 cm diameter in our case).

Correctly measuring the thermal emittance on smaller samples will allow for the deposition of SSA with a better thickness uniformity and avoid such uncertainty.

To reduce the minimal dimension required to correctly measure the extremely low thermal emittance in newly developed SSA, the radiative and conductive contributions to the *ATL* have to be minimized. This can be achieved by reducing the irradiating surface (miniaturizing the thermocouple elements) and/or using low emittance material (i.e., by adding a copper layer on the bolt and nut used to connect the thermocouple) and adopting extremely low conductive materials (such as ceramic) to support the sample.

5. Conclusions

The manuscript presents significant advances in measuring thermal emittance for extremely low-emissive materials, which are essential to correctly assess the energy conversion efficiency in newly developed Selective Solar Absorbers (SSAs). The methodology enables accurate measurement of thermal emittance values for copper samples, addressing the limitations posed by sample size. The measured copper thermal emittance values align closely with the literature data, underscoring the method's effectiveness in measuring thermal emittance values below 0.02 with a precision better than 0.003.

Also, the relation between the sample dimensions and minimal thermal emittance measurable value has been highlighted, and indications to further reduce the minimal measurable sample dimensions have been provided. Reducing the bold and nut dimensions from M3 to M2 would reduce the emitting surface by about a factor of two, and a factor of three can be obtained by coating the stainless steel bolt and nut with a copper film, resulting in a minimal dimension of about 8 cm^2 to measure thermal emittance values of 0.02. The new system will allow for determining the thermal emittance of SSA deposited on Cu samples with dimensions of 3x3 cm^2, eliminating the non-uniformity problem present in R&D deposition systems, which are often limited to dimensions below 5 cm in diameter (two inches).

Our findings are essential for correctly assessing the radiative properties in materials with very low thermal emittance, such as SSA for HVFPCs, and determining the energetic performance of the HVFPCs equipped with the new SSAs also in previously produced and measured SSAs.

Looking forward, the manuscript extends the applicability of this method to a broader range of materials and dimensions, enhancing the precision and utility of thermal emittance measurements in solar thermal applications where the radiative properties of SSA are fundamental in determining solar conversion efficiency.

CRediT authorship contribution statement

Eliana Gaudino: Writing – original draft, Visualization, Data curation. **Umar Farooq:** Investigation. **Antonio Caldarelli:** Validation, Data curation. **Paolo Strazzullo:** Investigation. **Daniela De Luca:** Visualization, Methodology. **Emiliano Di Gennaro:** Writing – review & editing, Supervision. **Roberto Russo:** Writing – review & editing, Supervision, Conceptualization. **Marilena Musto:** Writing – review &

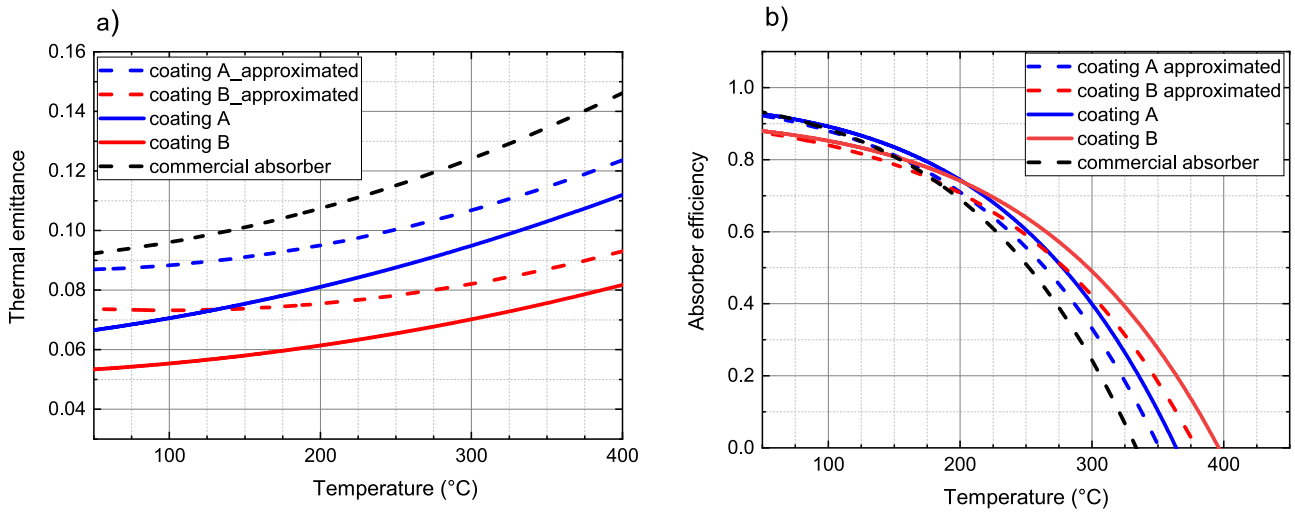

Fig. 6. a) measured absorber emittance using the mini test box at temperatures up to 400 °C for the commercial absorber (black line), Coating A (blue line), and Coating B (red line). The dashed lines represent the approximated values, while the continuous lines depict the values obtained considering the *ATL* term in the calorimetric balance equation; b) Calculated absorber efficiency for Mirotherm (black line), Coating A (blue line), and Coating B (red line). (For interpretation of the references to color in this figure legend, the reader is referred to the web version of this article.)

editing, Supervision, Methodology.

Declaration of competing interest

The authors declare that they have no known competing financial interests or personal relationships that could have appeared to influence the work reported in this paper.

Acknowledgment

This study was supported by the Eurostar Program powered by EUREKA and co-funded by the European Union and MUR (Ministry of Universities and Research of Italy) (Project ESSTEAM reference E! 115642, CUP B69J21036070005).

References

[1] P. Ablewski, M. Bober, M. Zawada, Emissivities of vacuum compatible materials: towards minimising blackbody radiation shift uncertainty in optical atomic clocks at room temperatures, Metrologia 57 (2020) 035004, https://doi.org/10.1088/1681-7575/ab63ae.
[2] A. Caldarelli, C. D'Alessandro, D. De Maio, D. De Luca, E. Gaudino, M. Musto, E. Di Gennaro, R. Russo, Characterization and thermal aging tests of Cr based multilayer for unconcentrated solar thermal applications, Thin Solid Films 735 (2021) 138870, https://doi.org/10.1016/j.tsf.2021.138870.
[3] A. Caldarelli, E. Gaudino, D. De Luca, U. Farooq, M. Musto, E. Di Gennaro, R. Russo, Low emissivity thin film coating to enhance the thermal conversion efficiency of selective solar absorber in high vacuum flat plate collectors, Thin Solid Films 764 (2023) 139632, https://doi.org/10.1016/j.tsf.2022.139632.
[4] F. Cao, K. McEnaney, G. Chen, Z. Ren, A review of cermet-based spectrally selective solar absorbers, Energy Environ. Sci. 7 (2014) 1615, https://doi.org/10.1039/c3ee43825b.
[5] F. Cao, L. Tang, Y. Li, A.P. Litvinchuk, J. Bao, Z. Ren, A high-temperature stable spectrally-selective solar absorber based on cermet of titanium nitride in SiO2 deposited on lanthanum aluminate, Sol. Energy Mater. Sol. Cells 160 (2017) 12–17, https://doi.org/10.1016/j.solmat.2016.10.012.
[6] S.X. Cheng, Total hemispherical emissivities of cobalt and nickel in the range 350–1000 K, Exp. Therm Fluid Sci. 2 (1989) 165–172, https://doi.org/10.1016/0894-1777(89)90030-7.
[7] C. D'Alessandro, D. De Maio, A. Caldarelli, M. Musto, F. Di Giamberardino, M. Monti, T. Mundo, E. Di Gennaro, R. Russo, V.G. Palmieri, Calorimetric testing of solar thermal absorbers for high vacuum flat panels, Sol. Energy 243 (2022) 81–90, https://doi.org/10.1016/j.solener.2022.07.039.
[8] P. Das, S. Rudra, K.C. Maurya, B. Saha, Ultra-emissive MgO-PVDF polymer nanocomposite paint for passive daytime radiative cooling, Adv. Mater. Technol. (2023) 2301174, https://doi.org/10.1002/admt.202301174.
[9] D. De Maio, C. D'Alessandro, A. Caldarelli, D. De Luca, E. Di Gennaro, R. Russo, M. Musto, A selective solar absorber for unconcentrated solar thermal panels, Energies 14 (2021) 900, https://doi.org/10.3390/en14040900.
[10] D. De Maio, C. D'Alessandro, A. Caldarelli, D. De Luca, E.D. Gennaro, M. Casalino, M. Iodice, M. Gioffre, R. Russo, M. Musto, Multilayers for efficient thermal energy conversion in high vacuum flat solar thermal panels, Thin Solid Films 735 (2021) 138869, https://doi.org/10.1016/j.tsf.2021.138869.
[11] D. De Maio, C. D'Alessandro, A. Caldarelli, M. Musto, R. Russo, Solar selective coatings for evacuated flat plate collectors: Optimisation and efficiency robustness analysis, Sol. Energy Mater. Sol. Cells 242 (2022) 111749, https://doi.org/10.1016/j.solmat.2022.111749.
[12] E. Gaudino, A. Caldarelli, R. Russo, M. Musto, Formulation of an efficiency model valid for high vacuum flat plate collectors, Energies 16 (2023) 7650, https://doi.org/10.3390/en16227650.
[13] N. Herguedas, E. Carretero, Evaluation of low-emissivity coatings with single, double, and triple silver layers, Sol. Energy Mater. Sol. Cells 263 (2023) 112592, https://doi.org/10.1016/j.solmat.2023.112592.
[14] B.P. Jelle, S.E. Kalnæs, T. Gao, Low-emissivity materials for building applications: a state-of-the-art review and future research perspectives, Energ. Build. 96 (2015) 329–356, https://doi.org/10.1016/j.enbuild.2015.03.024.
[15] X. Jiang, T. Wang, Q. Zhong, R. Yan, X. Huang, A near-ideal solar selective absorber with strong broadband optical absorption from UV to NIR, Nanotechnology 31 (2020) 315202, https://doi.org/10.1088/1361-6528/ab88ee.
[16] S.Y. Lee, N. Mettlach, N. Nguyen, Y.M. Sun, J.M. White, Copper oxide reduction through vacuum annealing, Appl. Surf. Sci. 206 (2003) 102–109, https://doi.org/10.1016/S0169-4332(02)01239-4.
[17] S. Mahmoudinezhad, M. Sadi, H. Ghiasirad, A. Arabkoohsar, A comprehensive review on the current technologies and recent developments in high-temperature heat exchangers, Renew. Sustain. Energy Rev. 183 (2023) 113467, https://doi.org/10.1016/j.rser.2023.113467.
[18] S.-T. Mi, Y.-C. Zhang, X.-B. Fu, Q. Li, T. Kong, Study on infrared emissivity model based on perturbation method and Kirchhoff approximation and its application in aluminum alloy welding, Optik 290 (2023) 171347, https://doi.org/10.1016/j.ijleo.2023.171347.
[19] C. Monte, B. Gutschwager, S.P. Morozova, J. Hollandt, Radiation thermometry and emissivity measurements under vacuum at the PTB, Int. J. Thermophys. 30 (2009) 203–219, https://doi.org/10.1007/s10765-008-0442-9.
[20] Z.Y. Nuru, D.E. Motaung, K. Kaviyarasu, M. Maaza, Optimization and preparation of Pt–Al2O3 double cermet as selective solar absorber coatings, J. Alloy. Compd. 664 (2016) 161–168, https://doi.org/10.1016/j.jallcom.2015.12.201.
[21] K.K. Phani Kumar, S.R. Atchuta, M. Shiva Prasad, H.C. Barshilia, S. Sakthivel, Review on selective absorber coatings: a catalyst for enhanced solar energy conversion efficiency, Sol. Energy Mater. Sol. Cells 277 (2024) 113080, https://doi.org/10.1016/j.solmat.2024.113080.
[22] S. Pratesi, M. De Lucia, M. Meucci, E. Sani, Structural and optical properties of copper-coated substrates for solar thermal absorbers, Superlattice. Microst. 98 (2016) 342–350, https://doi.org/10.1016/j.spmi.2016.08.031.
[23] Querry, M.R., 1985. Optical constants, Contractor Report.
[24] K.G. Ramanathan, S.H. Yen, E.A. Estalote, Total hemispherical emissivities of copper, aluminum, and silver, Appl. Opt. 16 (1977) 2810, https://doi.org/10.1364/AO.16.002810.
[25] R. Russo, M. Monti, F. di Giamberardino, V.G. Palmieri, Characterization of selective solar absorber under high vacuum, Opt. Express 26 (2018) A480, https://doi.org/10.1364/OE.26.00A480.
[26] P.A. Van Nijnatten, M.G. Hutchins, N.B. Kilbey, A. Roos, K. Gelin, F. Geotti-Bianchini, P. Polato, C. Anderson, F. Olive, M. Köhl, R. Spragg, P. Turner, Uncertainties in the determination of thermal emissivity by measurement of reflectance using Fourier transform spectrometers, Thin Solid Films 502 (2006) 164–169, https://doi.org/10.1016/j.tsf.2005.07.262.
[27] C.-D. Wen, I. Mudawar, Modeling the effects of surface roughness on the emissivity of aluminum alloys, Int. J. Heat Mass Transf. 49 (2006) 4279–4289, https://doi.org/10.1016/j.ijheatmasstransfer.2006.04.037.
[28] J. Xu, J. Wang, L. Lu, M. Gao, Study on the infrared emissivity of nonstoichiometric titanium chromium nitride films, Thin Solid Films 754 (2022) 139303, https://doi.org/10.1016/j.tsf.2022.139303.
[29] K. Xu, L. Hao, M. Du, J. Mi, Q. Yu, S. Li, J. Wang, S. Li, Thermal emittance of Ag films deposited by magnetron sputtering, Vacuum 174 (2020) 109200, https://doi.org/10.1016/j.vacuum.2020.109200.
[30] D. Yang, X. Zhao, Y. Liu, J. Li, H. Liu, X. Hu, Z. Li, J. Zhang, J. Guo, Y. Chen, B. Yang, Enhanced thermal stability of solar selective absorber based on nano-multilayered AlCrSiO films, Sol. Energy Mater. Sol. Cells 207 (2020) 110331, https://doi.org/10.1016/j.solmat.2019.110331.
[31] K. Yu, G. Wang, L. Li, K. Zhang, Y. Liu, A new experimental apparatus for polarized spectral emissivity measurement in a controlled environment, Infrared Phys. Technol. 111 (2020) 103572, https://doi.org/10.1016/j.infrared.2020.103572.
[32] K. Zhang, Y. Xu, X. Wu, K. Yu, Y. Liu, A new approach for accurately measuring the spectral emissivity via modulating the surrounding radiation, J. Quant. Spectrosc. Radiat. Transf. 288 (2022) 108277, https://doi.org/10.1016/j.jqsrt.2022.108277.
[33] K. Zhang, Y. Zhao, K. Yu, Y. Liu, Development of experimental apparatus for precise emissivity determination based on the improved method compensating disturbances by background radiation, Infrared Phys. Technol. 92 (2018) 350–357, https://doi.org/10.1016/j.infrared.2018.06.031.
[34] W.J. Zhang, J. Qiu, L.H. Liu, Deviation characteristics of specular reflectivity of micro-rough surface from Fresnel's equation, J. Quant. Spectrosc. Radiat. Transf. 160 (2015) 50–62, https://doi.org/10.1016/j.jqsrt.2015.03.023.
[35] W.-W. Zhang, H. Qi, Z.-Q. Yu, M.-J. He, Y.-T. Ren, Y. Li, Optimization configuration of selective solar absorber using multi-island genetic algorithm, Sol. Energy 224 (2021) 947–955, https://doi.org/10.1016/j.solener.2021.06.059.